Journal of Physics B: Atomic, Molecular and Optical Physics

PAPER

Spectroscopic analysis of N-intrashell transitions in Rb-like to Ni-like Yb ions

To cite this article: Dipti *et al* 2020 *J. Phys. B: At. Mol. Opt. Phys.* **53** 145002

IOP Publishing Journal of Physics B: Atomic, Molecular and Optical Physics
J. Phys. B: At. Mol. Opt. Phys. **53** (2020) 145002 (14pp) https://doi.org/10.1088/1361-6455/ab8716

Spectroscopic analysis of N-intrashell transitions in Rb-like to Ni-like Yb ions

Dipti[1,5], R Silwal[1,2,3], J M Dreiling[1,4], S C Sanders[1,2], E Takacs[1,2] and Yu Ralchenko[1,5]

[1] National Institute of Standards and Technology, Gaithersburg, MD 20899, United States of America
[2] Department of Physics and Astronomy, Clemson University, Clemson, SC 29634, United States of America

E-mail: fnu.dipti@nist.gov and yuri.ralchenko@nist.gov

Received 28 January 2020, revised 22 March 2020
Accepted for publication 6 April 2020
Published 9 June 2020

Abstract

Extreme ultraviolet spectra of highly-charged ytterbium ions produced in an electron beam ion trap at the National Institute of Standards and Technology were observed with a flat-field grazing incidence spectrometer in the wavelength region of about 4 nm–20 nm. The measured spectra were interpreted through detailed analysis by collisional-radiative modeling of the non-Maxwellian EBIT plasma. Seventy-nine new spectral lines due to intrashell ($\Delta n = 0$, $n = 4$) electric–dipole, magnetic–dipole, and electric–quadrupole transitions were identified in Rb-like Yb^{33+} through Ni-like Yb^{42+} ions. The effects of strong configuration interaction within the $n = 4$ complex on the measured spectra are discussed for a number of ionization stages.

Keywords: spectroscopy, electron beam ion trap, highly-charged ions, ytterbium, collisional-radiative modeling

(Some figures may appear in colour only in the online journal)

1. Introduction

The importance of rare-earth (RE) elements in modern technology and science is well appreciated. From quantum optics to astrophysics, from nanotechnolo gy to nuclear physics, from applied research to fundamental physics, RE elements are utilized to create new materials, to explore explosive astrophysical events (e.g. neutron star mergers [1]), and to test the most advanced atomic theories. While most of the spectroscopic research on RE elements is aimed at neutral or low-charged ions, the last several decades witnessed significant growth of studies of their highly-charged ions.

The spectra of highly-charged ions of rare-earth elements in the extreme ultraviolet (EUV) and soft x-ray ranges are highly important in fundamental research as well as industrial applications such as plasma diagnostics, soft x-ray lasers, and the next generation lithography sources [2]. To this end, spectra of a number of RE elements have been investigated in laser-produced plasmas (LPPs) [3–7], electron beam ion traps (EBITs) [8], tokamaks [9], and stellarators [10–12]. In particular, the EBIT facility at the National Institute of Standards and Technology (NIST) [13, 14] has been used to analyze the spectra from the N-shell ions of several RE elements including Sm, Gd, Dy, and Er [15–18]. These studies have resulted in identification of hundreds of new spectral lines and energy levels that significantly improved our understanding of atomic structure and diagnostic potential of RE ions.

Spectroscopy of ytterbium (Yb, $Z = 70$) has also been a subject of extensive research. This element is used in promising applications, such as very precise optical lattice clocks [19, 20], scintillators [21], and solid state lasers [22], and therefore, there are dozens of research papers discussing various atomic and spectroscopic properties of neutral and low-charged Yb. As for highly-charged Yb, the available atomic data are rather restricted. Existing measurements are mainly for Cu-like and Zn-like isoelectronic sequences from

[3] Present address: TRIUMF, 4004 Wesbrook Mall, Vancouver, BC V6T 2A3, Canada.
[4] Present address: Honeywell Quantum Solutions, Broomfield, CO 80021, United States of America.
[5] Authors to whom any correspondence should be addressed.

experiments with EBITs [23–25], LPPs [26–32], tokamaks [29, 33, 34], and the large helical device (LHD) stellarator [12]. A few isolated lines from Ga-like and Ni-like ytterbium and neighboring heavy ions were also reported from laser-produced plasmas [9, 35, 36]. On the other hand, there is a rich set of theoretical papers on Yb spectroscopy (see, e.g. [37]) that can be benchmarked by precise measurements of EUV and x-ray spectra from highly-charged ions of Yb.

To address this situation, we extend our previous EUV measurements of N-shell rare-earth ions to Yb. Particularly, we report the measured spectra from Rb-like Yb^{33+} through Ni-like Yb^{42+} ions as well as identify the newly recorded spectral lines based upon large-scale collisional-radiative modeling of the EBIT plasma emission. Additionally, detailed comparisons of the experimental data with our calculations and other works are provided.

2. Experimental approach

For the present work, the NIST EBIT was used to produce and trap highly-charged Yb ions. In the EBIT, an intense electron beam emitted by a high perveance electron gun is accelerated toward the trap region that consists of three drift tube electrodes. The acceleration is caused by the potential difference between the cathode in the gun and the center drift tube in the trap. This potential difference defines the electron beam energy, which is lowered by the space charge of the electron beam. The electron beam is compressed to a few tens of microns by a superconducting magnet of 2.7 T surrounding the trap. The element of study is injected into the trap region either as a neutral gas [38] or as singly-charged ions from a metal vapor vacuum arc (MeVVA) ion source [39] which is situated on the top of the EBIT and floated at a potential of 10 kV.

During the measurement, singly-charged Yb ions injected from the MeVVA source were further ionized to highly-charged states by electron impact ionization. The potential of the center drift tube was matched to the MeVVA floating potential to capture the Yb ions. The ions were then confined axially by the electric field applied to the three cylindrical drift tubes and radially by the space charge of the electron beam and the 2.7 T axial magnetic field. The details of the MeVVA ions capture and trapping scheme is provided in reference [40].

The electron beam energy was varied between 1.61 keV and 3.21 keV during the measurement, based on the ionization energies of the charge states of interest. This electron beam energy is given by the electronic charge times the potential difference between the electron gun cathode and the center drift tube, lowered by the space charge potential of the electron beam. The electron beam current ranged between 57 mA and 90 mA as the beam energy changed. The emissions from the highly-charged Yb plasma in the EUV region were recorded by a flat-field grazing incidence EUV spectrometer with a resolution of 0.03 nm at 30 nm wavelength [41]. The light from the EBIT plasma is dispersed by a reflection grating of 1200 grooves/mm and imaged onto a liquid-nitrogen-cooled 2D CCD camera.

Ten 60 s frames of EUV spectra were collected at each beam energy such that the total acquisition time was 600 s each. The EUV spectrum recorded in the 2D CCD pixels was hardware binned to a 1D spectrum. A cosmic ray removal routine was implemented to clean the spectra prior to the spectral analysis as discussed in reference [40]. To convert the spectral range in pixel number to wavelength in nm, well-known lines from highly-charged Ne, Fe, Xe, and Ba ions [37, 42] were used. These calibration lines were first fit with a Gaussian function to get the peak position. The literature wavelength values were then plotted as a function of pixel positions and fitted by a weighted third-order polynomial. The weight included a total uncertainty that is a combination of the literature uncertainty, the uncertainty of the Gaussian fit of the calibration lines, and a constant systematic uncertainty of 0.0011 nm. This systematic uncertainty was obtained by requiring the reduced chi-square of the polynomial fit to be 1. The wavelength range for the current measurement was 4 nm–20 nm.

The measured spectra for Yb at nine beam energies are presented in figure 1. To aid in the identification of lines, the wavelengths are multiplied by a factor of 2 and 3, while the intensities are reduced by a factor of about 3 and 6 to obtain the second- and third-orders of the diffraction of the grating, respectively. The vertical shifted lines show the prediction of the second- and third- order spectra.

3. Collisional-radiative modeling

The radiation of the EBIT plasma was simulated using the non-Maxwellian collisional-radiative code NOMAD [43] in order to interpret the observed spectral features. The model includes twelve ion stages of Rb-like to Fe-like Yb ions and all the relevant atomic data such as level energies, radiative rates (dipole allowed as well as forbidden transitions), electron impact excitation (de-excitation), and ionization (recombination) as calculated by the flexible atomic code (FAC) [44]. The atomic structure calculations in the fine-structure mode were carried out for all singly-excited configurations up to $n = 6$ or 7 (depending upon the ion stage involved) and some doubly-excited configurations. This resulted in about 18 000 fine-structure levels.

For all ions except Br-like, Kr-like, and Rb-like ions, the energies of the fine-structure levels of the $n = 4$ configurations were substituted with values obtained with more extensive structure calculations including all possible excitations within the $n = 4$ shell. Due to the large number of energy levels in Br-like, Kr-like, and Rb-like ions, the energies were modified by considering triple excitations within the $n = 4$ shell. The energies in Cu-like and Zn-like ions were also corrected for single excitation from the 3p and 3d sub-shell to the $n = 4$ shell. The spectra, simulated with these energy modifications, match the experimental wavelengths better than the energies obtained with the singly- and doubly-excited configurations [17, 45]. The improvement is due to the inclusion of more valence–valence electron correlation in this approach. For example, the calculated wavelength of the resonance transition in Cu-like ion changes from 7.5237 nm to 7.5770 nm; the latter value with increased electron correlations is closer to

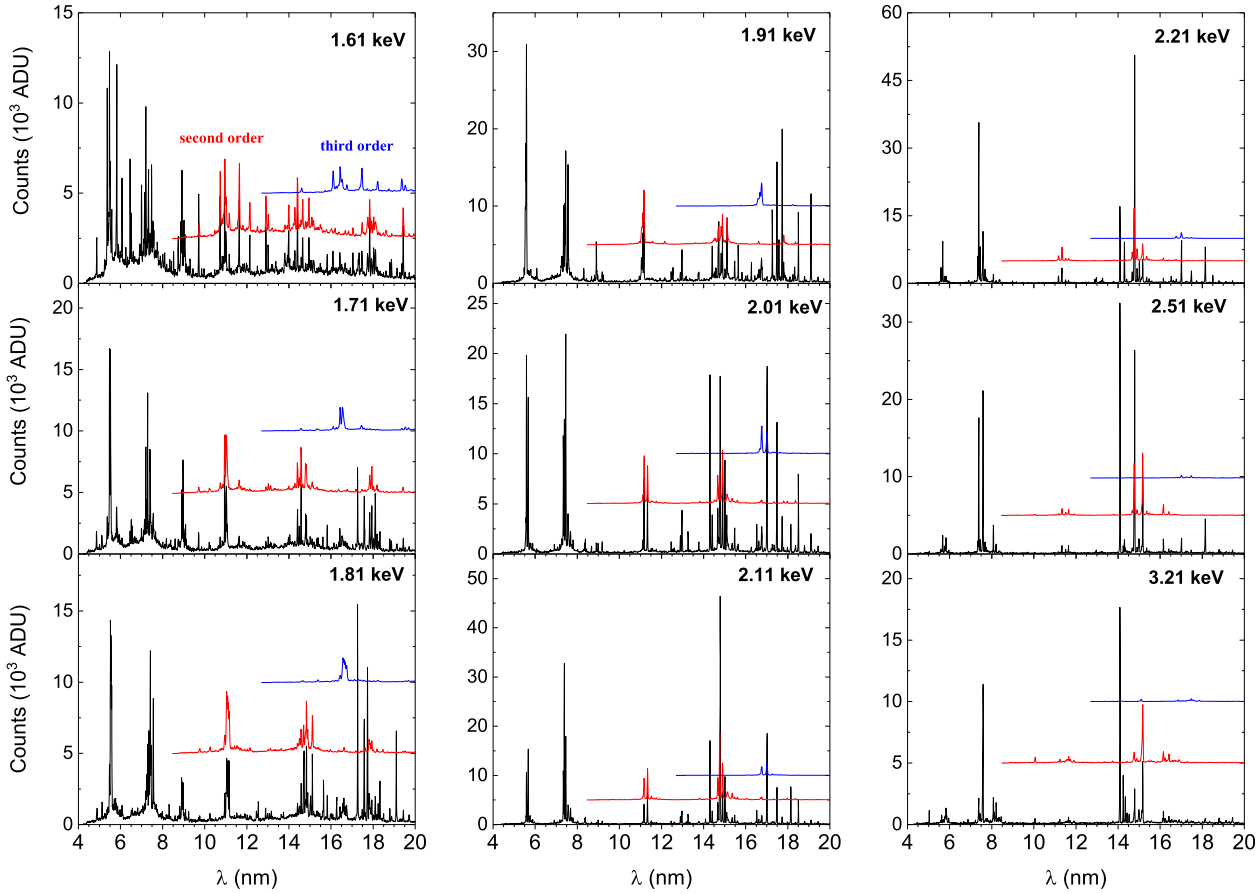

Figure 1. EUV spectra of Yb ions at nine beam energies between 1.61 keV and 3.21 keV in the wavelength region of 4 nm–20 nm. The spectrum counts are the analog-to digital units (ADU) of the CCD detector. The vertical shifted lines (red and blue) represent the second- and third-orders of diffraction, respectively.

the measured value of 7.5871(13) nm. For Ni-like Yb ions, we have used the energies of the $3d^9 4l$ configuration available from more accurate theoretical calculations using the relativistic many body perturbation theory (RMBPT) [46].

The charge exchange (CX) between ions and neutral particles in the trap is also included in our model through a variable parameter which is the product of two parameters: the density of neutrals and their relative velocity with respect to the ions. The spectra were modeled assuming an electron density of 10^{11} cm^{-3} and a Gaussian electron beam energy distribution of 40 eV full width at half maximum which approximately matches the conditions of the EBIT [47]. The calculated spectra were convolved with the spectrometer energy resolution and corrected for the efficiency of the grazing incidence instrument [41]. Although line identification is not sensitive to the space charge corrections to the electron beam energy, we have taken it into account to match the calculated intensity ratios with measurements. Space charge correction to electron beam energy was observed to be around 100 eV–200 eV in this regime of beam energies.

4. Results and discussion

In figure 2, we present the comparison of the experimental spectra at a nominal electron beam energy of 2.11 keV with the simulated spectra at energy 1.95 keV, which takes into account the aforementioned space charge correction. The second- and third-order spectra are represented explicitly in the experimental spectra by the vertical shifted lines. We have also included the second- and third-order lines in the theoretical spectra. It can be clearly seen that the calculated line positions as well as the intensity ratios are in good agreement with the measured values. The spectra were produced mainly from As-, Ge-, Ga-, and Zn-like Yb ions (see figure 2(c)), whose calculated relative populations at this energy were 0.04, 0.19, 0.45, and 0.31, respectively, while the rest of the population was in lower ionization stages. The group of strong spectral lines near 5.6 nm, 7.4 nm, and 14 nm are due to E1 transitions $4\overline{p}-4\overline{d}$, 4s–4p, and 4s–$4\overline{p}$, respectively. (Here, we are representing the orbitals in standard relativistic notation with nl and $n\overline{l}$ having total angular momentum $j = l + 1/2$ and $j = l - 1/2$, respectively, where n is the principal quantum number, and l is the orbital quantum number.) Lines with wavelength greater than 16 nm are due to the forbidden M1 and E2 transitions $4\overline{p} - 4p$.

The very weak line at 5.8802(14) nm observed (see inset of figure 2(a)) in both experiment and theory is due to the transition between the configurations $4s4p^2$–$4s^24f$ in Ga-like Yb^{39+} ions. The observed line indicates strong mixing through configuration interaction among 4s4f–4p4d. In

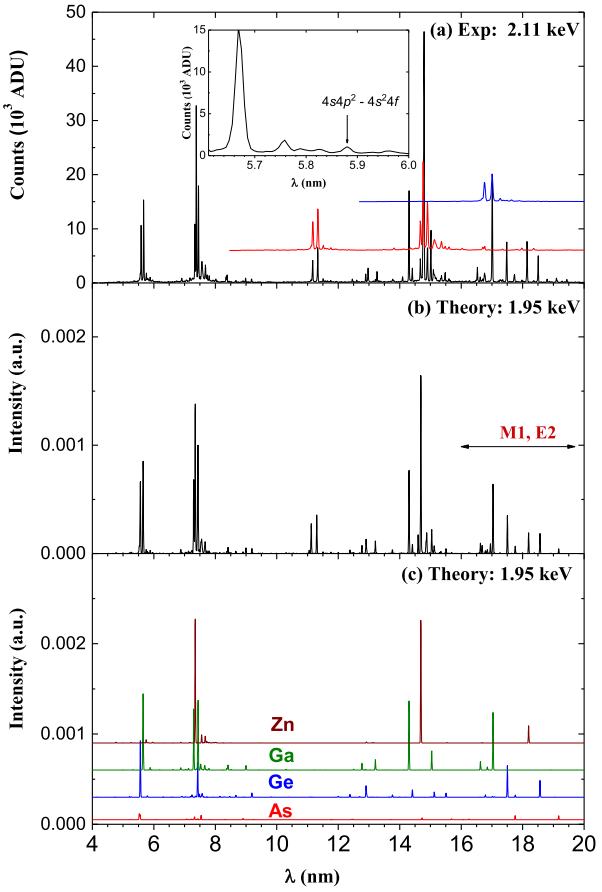

Figure 2. Comparison between the (a) measured spectra (in analog to digital units (ADU) of the detector) at an electron beam energy of 2.11 keV and (b) simulated spectra (in arbitrary units) at an electron beam energy of 1.95 keV. For the experimental spectra, the second- (red) and third-order (blue) of diffraction are shown in vertical offsets. The second- and third-order contributions are also included in the theoretical spectra. Lines in the longer wavelength region (>16 nm) are due to the forbidden M1 and E2 transitions. The inset in figure 2(a) shows the spectral features near the weak line at 5.8802(14) nm, which is due to the transition between the configurations $4s4p^2$–$4s^24f$ in Ga-like Yb^{39+} ions. (c) Spectra based on the collisional-radiative modeling for Zn-like, Ga-like, Ge-like, and As-like charge states at an electron beam energy of 1.95 keV.

table 1, we have given the major contributions to the lower ($4s4p^2$) and upper ($4s^24f$) levels for the involved transition in Ga-like ion using FAC and GRASP2K [48] codes. In GRASP2K, the active space was expanded separately for even- and odd-parity states considering the single and double excitations from the occupied orbitals 3d, 4l (l = 0–3) to n = 5. Breit interaction and quantum electrodynamics (QED) effects were also included as perturbations. The shells having closed shell configurations such as $4s^2$ and $4\overline{p}^2$ have zero total angular momentum and therefore are omitted from the table. We also omit the j value for shells with one hole, as the total angular momentum is equal to that of one electron in the shell. One can see from table 1 that both FAC and GRASP results are in excellent agreement and predict strong mixing among $4s^24f$ and 4s4p4d configurations. A similar weak transition was also observed at 5.7916(16) nm in Ge-like Yb^{38+} ions between $4s4p^3$–$4s^24p4f$. Strong configuration interactions through 4s4f–4p4d and 4p4f–$4d^2$ can shift the width of the transition array and the intensities for $\Delta n = 0$ transitions in N-shell ions and, therefore, should be taken into account [49].

The spectral lines were identified by comparing the theoretical spectra with the measured ones, and the line positions have been listed in table 2 along with the theoretical results obtained using FAC. Although configuration mixing is strong for the involved transitions, we list the dominant lower and upper levels in table 2. The FAC level numbering is also provided in the square brackets to avoid any ambiguity for the lower and upper levels.

4.1. Rb-like Yb^{33+} through As-like Yb^{37+}

No previous experimental or theoretical study has been reported for Rb-like through As-like Yb ions. Strong EUV emission is observed from these charge states for a beam energy range of 1.61 keV and 1.91 keV, which is slightly greater than the ionization energy of Rb-like and As-like Yb (1.324 keV and 1.668 keV, respectively) [37]. The weak spectral lines from As-like are also visible at the nominal beam energy of 2.01 keV. The most intense spectral features originate from transitions between the ground $4p^k4d^n$ (k = 3–6, n = 0, 1) and the first-excited configuration $4p^{k-1}4d^{n+1}$. Transitions between the ground and the first-excited configuration give rise to strong EUV emission which splits into four regions due to the spin–orbit interaction. For example, in the Rb-like Yb^{33+} ion, the transitions around 5.6 nm, 7.3 nm, and 8.9 nm are due to $4\overline{p}$–$4\overline{d}$ ($\Delta J = 1$), 4p–4d ($\Delta J = 1$), and 4p–$4\overline{d}$ (ΔJ = 0), respectively. The weak transition $4\overline{p} - 4d$ ($\Delta J = 2$) is not observed in the measured spectra. The transition $4\overline{d} - 4\overline{f}$ ($\Delta J = 1$) falls at a wavelength in between the $4\overline{p} - 4\overline{d}$ and 4p–4d transitions. With increasing ion charge, the line position for the same transition moves systematically toward the longer wavelength region. As some of the lines are not well isolated, the change in the ion charge distribution at different beam energies can be used to help identify lines from different charge states. The second-order spectra have also been utilized for the unambiguous identification of strong lines. For example, the line observed at 5.4788(18) nm for $E_b = 1.61$ keV is identified to be from the $4p^6$–$4p^5$4d transition in Kr-like Yb. At E_b = 1.71 keV, the line at the same wavelength corresponds to a blend of lines from Kr-like and Br-like ions. Therefore, we have used the higher nominal beam energies of 1.81 keV and 1.91 keV to determine the wavelength of the transition in Br-like ion where no Kr-like ions are present. In addition to the transition from the valence 4p sub-shell, a single line from 4s at 7.2488(23) nm was also observed in Br-like ion. We have identified three transitions at 12.5452(12) nm, 14.7125(20) nm, and 15.6464(13) nm in As-like ions due to the 4s–$4\overline{p}$ transition. Only M1 forbidden transitions ($4\overline{p} - 4p$) within the low-lying levels of Kr-like through As-like ions were observed in the longer wavelength region (>16 nm). In total, we have identified 49 new lines in Rb-like through As-like Yb ions, out of which seven are blended lines.

FAC calculated wavelengths are available for comparison with the measured values and are shown in figure 3. The dashed lines in the figure represent the experimental

Table 1. Mixing coefficients of $(4s4p^2)_{3/2}$ and $(4s^24f)_{5/2}$ in Ga-like Yb ion.

State	Method	Major contributions
$(4s4p^2)_{3/2}$	FAC	68.4% $(4s4\overline{p})_1 4p$ + 25.3% $(4s4\overline{p})_0 4p$ + 4.1% $4\overline{d}$ + 1.6% $4s(4p^2)_2$
	GRASP	68.4% $(4s4\overline{p})_1 4p$ + 25.4% $(4s4\overline{p})_0 4p$ + 3.8% $4\overline{d}$ + 1.5% $4s(4p^2)_2$
$(4s^24f)_{5/2}$	FAC	51.6% $4\overline{f}$ + 42.3% $(4s4p)_1 4\overline{d}$ + 1.8% $(4s4p)_1 4d$ + 1.4% $(4s4p)_2 4\overline{d}$ + 1.0% $4\overline{p}(4p^2)_2$
	GRASP	51.0% $4\overline{f}$ + 42.0% $(4s4p)_1 4\overline{d}$ + 1.8% $(4s4p)_1 4d$ + 1.6% $(4s4p)_2 4\overline{d}$ + 1.3% $4\overline{p}(4p^2)_2$ + 1.0% $(4s4p)_2 4d$

uncertainties in the wavelengths as listed in table 2 for each individual identified line. The calculated wavelengths are mostly shorter than the measured values for the shorter wavelength region. However, for the low-lying levels giving rise to the 4s–$4\overline{p}$ and $4\overline{p}$ –4p transitions, our calculated wavelengths are longer than the measured ones. The different behavior (for the transitions between low-lying levels and those involving the excited configurations) may be due to the optimization of the radial potential, as we have only used the ground configuration for the optimization. The 4s–$4\overline{p}$ transition at 12.5452(12) nm showed a relatively larger discrepancy between the measured and theoretical wavelengths as compared to other lines shown in figure 3. The core ($1s^22s^22p^63s^23p^63d^{10}$) and valence ($n = 4$) correlations, which were not included in the atomic structure calculations, may have a more pronounced effect on transitions involving 4s orbitals as compared to 4p and 4d. The 4s–$4\overline{p}$ transition is not observed in Rb-, Kr-, Br-, and Se-like ions. Overall, our experimental and FAC calculated wavelengths are found to agree within 1%.

4.2. Ge-like Yb^{38+}

Experimentally determined wavelengths for eleven dipole-allowed transitions between the $4s^24p^2$–$4s^24p4d$, $4s^24p^2$–$4s4p^3$, $4s4p^3$–$4s^24p4f$, $4s4p^3$–$4s4p^24d$, and $4s^24p4d$–$4s4p^24d$ configurations are listed in table 2. In addition, two forbidden lines (E2 and M1) within the configuration $4s^24p^2$ were also observed in the recorded emission. Only the theoretical calculations of Palmeri *et al* [50] and the present FAC results are available for comparison. Palmeri *et al* [50] carried out fully-relativistic multiconfiguration Dirac–Fock (MCDF) calculations by using the GRASP code and reported wavelengths and transition probabilities for the $4s^24p^2$–$4s4p^3$ and $4s^24p^2$–$4s^24p4d$ transitions in Ge-like heavy ions. They have adjusted their calculated values by fitting the difference between the theoretical and the few experimental wavelength values available along the isoelectronic sequence by a function quadratic in $1/Z$. Their corrected wavelengths of 5.5903 nm and 7.4473 nm for transitions $(4\overline{p}^2)_0$–$(4\overline{p}4\overline{d})_1$ and $(4\overline{p}^2)_0$–$(4s4p)_1$, respectively, are close to our measured wavelengths. Overall, the agreement of the FAC and MCDF results [50] to the measured wavelengths is within 0.6%.

4.3. Ga-like Yb^{39+}

We have identified 11 new lines in Ga-like ions and three previously reported from the spectra of low-density tokamak and high-density laser-produced plasmas [9]. Our measured wavelengths for the 4s–4p transitions at 7.3376(12) nm and 7.4528(12) nm agree with the low-resolution results of Fournier *et al* [9]. However, the line at 5.6694(15) nm due to the $4\overline{p} - 4\overline{d}$ transition disagrees with their value of 5.74 nm detected in a tokamak plasma [9]. Using the parametric potential code RELAC, they also reported a theoretical wavelength of 5.608 nm, which is closer to our measured wavelength than their measurement of 5.74 nm. Our measured wavelengths for these three transitions are in excellent agreement with the calculations of Fan *et al* [51], which employed GRASP2K code to determine the energy levels and the transition probabilities for $4s^24p$, $4s4p^2$, and $4s^24d$ configurations of Ga-like ions. Their calculations also showed excellent agreement with the high-precision EBIT measurements of the $4\overline{p} - 4\overline{d}$ transition in W, Os, and Au ions, which further establishes the reliability of the calculations. The wavelength of the resonance transition in Ga-like ions was also reported by Hu *et al* [52] using GRASP, which agrees to within 0.09% of our wavelength. Quinet *et al* [53] also used GRASP to calculate the wavelengths of the dipole allowed ($4s^24p$–$4s^24d$ and $4s^24p$–$4s4p^2$) and forbidden M1 and E2 transitions within the ground state configuration $4s^24p$, with reduced electron correlations compared to Fan *et al* [51]. Their results exhibit reasonable agreement with our measured wavelengths. The fine-structure splitting of the ground configuration $4s^24p$ gives rise to a forbidden M1 line at 17.0124(13) nm, which has been previously studied theoretically [53–56]. RMBPT calculations from Safronova *et al* [54] and semi-empirical calculations of Curtis [56] are in very good agreement with the measured value.

4.4. Zn-like Yb^{40+}

All the lines identified for Zn-like Yb^{40+} in the present work were previously reported in the literature except for the line at 7.6810(12) nm, which shows significant blending with the line at 7.6786(12) nm from Ga-like ion. The Zn-like line was identified at a beam energy of 2.51 keV where there was no contribution from the Ga-like ion. Previous experimental studies include the analysis of spectra of Zn-like ions produced in EBITs [24], LPPs [26, 30, 32], and the Princeton Large Torus (PLT) tokamak discharges [34]. More effort has been devoted toward high-precision atomic structure calculations of Zn-like heavy ions than to experimental results. Recently Hao and Liu [57] reported the fully-relativistic calculations with the multiconfiguration Dirac–Fock and general matrix element (MCDFGME) program which included Breit and QED effects. Vilkas and Ishikawa [58] performed calculations within the multireference Møllr–Plesset (MR–MP) formalism; while Träbert *et al* [59] applied the same approach with a larger basis set. Blundell *et al* [60] reported results using second-order RMBPT and

Table 2. Wavelengths (in nm) of the spectral lines of highly-charged ions of Yb. The numbers in square brackets are the number of lower and upper levels of FAC calculations. The numbers in parenthesis are the wavelength uncertainties in the unit of the last significant digit.

	Lower level		Upper level		λ_{Present}		$\lambda_{\text{Previous}}$		
Ion	Conf.	State	Conf.	State	Exp.	FAC	Exp.	Theory	Type
33 [Rb]	4d [1]	$(4\bar{d})_{3/2}$	$4p^5 4d^2$ [41]	$(4\bar{p}(4\bar{d})_2)_{3/2}$	5.3685(17)	5.3121			
33 [Rb]	4d [1]	$(4\bar{d})_{3/2}$	$4p^5 4d^2$ [40]	$(4\bar{p}(4\bar{d}^2)_0)_{1/2}$	5.5065(18)	5.4617			
33 [Rb]	4d [1]	$(4\bar{d})_{3/2}$	$4p^5 4d^2$ [34]	$(4\bar{p}(4\bar{d}^2)_2)_{5/2}$	5.8222(15)	5.7800			
33 [Rb]	4d [1]	$(4\bar{d})_{3/2}$	4f [32]	$(4\bar{f})_{5/2}$	6.4551(13)	6.4158			
33 [Rb]	4d [1]	$(4\bar{d})_{3/2}$	$4p^5 4d^2$ [27]	$((4p^3 4\bar{d})_3 4d)_{1/2}$	6.9974(12)	6.9439			
33 [Rb]	4d [2]	$(4d)_{5/2}$	$4p^5 4d^2$ [30]	$(4p^3(4d^2)_4)_{5/2}$	7.1418(13)	7.0905			
33 [Rb]	4d [1]	$(4\bar{d})_{3/2}$	$4p^5 4d^2$ [24]	$((4p^3 4\bar{d})_3 4d)_{3/2}$	7.3282(12)	7.2853			
33 [Rb]	4d [1]	$(4\bar{d})_{3/2}$	$4p^5 4d^2$ [20]	$((4p^3 4\bar{d})_2 4d)_{5/2}$	7.4762(12)	7.4384			
33 [Rb]	4d [1]	$(4\bar{d})_{3/2}$	$4p^5 4d^2$ [17]	$((4p^3 4\bar{d})_3 4d)_{5/2}$	7.7706(16)	7.7168			
33 [Rb]	4d [1]	$(4\bar{d})_{3/2}$	$4p^5 4d^2$ [5]	$(4p^3(4\bar{d}^2)_2)_{5/2}$	8.8699(15)	8.8417			
33 [Rb]	4d [2]	$(4d)_{5/2}$	$4p^5 4d^2$ [6]	$(4p^3(4\bar{d}^2)_2)_{7/2}$	9.7155(12)	9.6765			
34 [Kr]	$4p^6$ [1]	$(4p^4)_0$	$4p^5 4d$ [13]	$(4\bar{p}4\bar{d})_1$	5.4788(18)	5.4300			
34 [Kr]	$4p^5 4d$ [4]	$(4p^3 4\bar{d})_3$	$4p^5 4f$ [63]	$(4p^3 4\bar{f})_4$	6.5104(13)	6.4419			
34 [Kr]	$4p^6$ [1]	$(4p^4)_0$	$4p^5 4d$ [9]	$(4p^3 4d)_1$	7.2040(12)	7.1570			
34 [Kr]	$4p^6$ [1]	$(4p^4)_0$	$4p^5 4d$ [3]	$(4p^3 4\bar{d})_1$	8.9189(13)	8.8997			
34 [Kr]	$4p^5 4d$ [4]	$(4p^3 4\bar{d})_3$	$4p^5 4d$ [10]	$(4\bar{p}4\bar{d})_2$	18.8744(13)	18.8858			M1
35 [Br]	$4p^5$ [1]	$(4p)_{3/2}$	$4p^4 4d$ [26]	$((4\bar{p}4p^3)_2 4\bar{d})_{5/2}$	5.4783(21)	5.4316			
35 [Br]	$4p^5$ [1]	$(4p)_{3/2}$	$4p^4 4d$ [25]	$((4\bar{p}4p^3)_2 4\bar{d})_{3/2}$	5.5187(17)[B]	5.4590			
35 [Br]	$4p^5$ [1]	$(4p)_{3/2}$	$4p^4 4d$ [24]	$((4\bar{p}4p^3)_2 4\bar{d})_{1/2}$	5.5187(17)[B]	5.4622			
35 [Br]	$4p^5$ [1]	$(4p)_{3/2}$	$4s4p^6$ [14]	$(4s)_{1/2}$	7.2488(23)	7.1881			
35 [Br]	$4p^5$ [1]	$(4p)_{3/2}$	$4p^4 4d$ [13]	$((4p^2)_2 4d)_{5/2}$	7.2902(12)	7.2273			
35 [Br]	$4p^5$ [1]	$(4p)_{3/2}$	$4p^4 4d$ [12]	$((4p^2)_2 4d)_{3/2}$	7.3954(14)	7.3367			
35 [Br]	$4p^5$ [1]	$(4p)_{3/2}$	$4p^4 4d$ [6]	$((4p^2)_2 4\bar{d})_{7/2}$	8.7408(12)	8.7533			
35 [Br]	$4p^5$ [1]	$(4p)_{3/2}$	$4p^4 4d$ [5]	$((4p^2)_2 4\bar{d})_{5/2}$	8.9680(13)	8.9224			
35 [Br]	$4p^5$ [1]	$(4p)_{3/2}$	$4p^4 4d$ [3]	$((4p^2)_2 4\bar{d})_{3/2}$	9.0903(14)	9.0434			
35 [Br]	$4p^5$ [2]	$(4\bar{p})_{1/2}$	$4p^4 4d$ [7]	$((4p^2)_0 4\bar{d})_{3/2}$	15.3912(13)	15.4010			
35 [Br]	$4p^5$ [1]	$(4p)_{3/2}$	$4p^5$ [2]	$(4\bar{p})_{1/2}$	18.1056(14)	18.1361			M1
36 [Se]	$4p^4$ [1]	$(4p^2)_2$	$4p^3 4d$ [30]	$((4\bar{p}(4p^2)_2)_{3/2}4\bar{d})_3$	5.5235(16)	5.4926			
36 [Se]	$4p^4$ [1]	$(4p^2)_2$	$4p^3 4d$ [29]	$((4\bar{p}(4p^2)_2)_{5/2}4\bar{d})_1$	5.5372(16)[B]	5.5039			
36 [Se]	$4p^4$ [1]	$(4p^2)_2$	$4p^3 4d$ [28]	$((4\bar{p}(4p^2)_2)_{5/2}4\bar{d})_2$	5.5372(16)[B]	5.5050			
36 [Se]	$4p^4$ [1]	$(4p^2)_2$	$4p^3 4d$ [14]	$(4p4d)_3$	7.4168(13)[B]	7.3872			
36 [Se]	$4p^4$ [1]	$(4p^2)_2$	$4p^3 4d$ [13]	$(4p4d)_2$	7.4168(13)[B]	7.3881			
36 [Se]	$4p^4$ [4]	$(4\bar{p}4p^3)_2$	$4p^3 4d$ [10]	$(4p4d)_2$	15.8235(13)	15.8610			
36 [Se]	$4p^4$ [1]	$(4p^2)_2$	$4p^4$ [4]	$(4\bar{p}4p^3)_2$	17.2668(12)	17.2688			M1
36 [Se]	$4p^4$ [4]	$(4\bar{p}4p^3)_2$	$4p^3 4d$ [8]	$(4p4\bar{d})_3$	17.5774(12)	17.5312			
36 [Se]	$4p^3 4d$ [8]	$(4p4\bar{d})_3$	$4p^3 4d$ [20]	$((4\bar{p}(4p^2)_2)_{5/2}4\bar{d})_4$	18.2408(13)[B]	18.2474			M1
36 [Se]	$4p^3 4d$ [11]	$(4p4d)_4$	$4p^3 4d$ [26]	$((4\bar{p}(4p^2)_2)_{5/2}4d)_4$	18.2408(13)[B]	18.2476			M1
36 [Se]	$4p^4$ [1]	$(4p^2)_2$	$4p^4$ [3]	$(4\bar{p}4p^3)_1$	18.3256(13)	18.3668			M1

Table 2. Continued.

	Lower level		Upper level		λ_{Present}		$\lambda_{\text{Previous}}$		
Ion	Conf.	State	Conf.	State	Exp.	FAC	Exp.	Theory	Type
37 [As]	$4p^3$ [1]	$(4p)_{3/2}$	$4p^24d$ [20]	$((4\overline{p}4p)_2 4\overline{d})_{3/2}$	5.5556(16)[B]	5.5266			
37 [As]	$4p^3$ [1]	$(4p)_{3/2}$	$4p^24d$ [19]	$((4\overline{p}4p)_2 4\overline{d})_{1/2}$	5.5556(16)[B]	5.5283			
37 [As]	$4p^3$ [1]	$(4p)_{3/2}$	$4p^24d$ [18]	$((4\overline{p}4p)_1 4\overline{d})_{5/2}$	5.5792(16)	5.5541			
37 [As]	$4p^3$ [1]	$(4p)_{3/2}$	$4p^24d$ [12]	$((4\overline{p}4p)_2 4\overline{d})_{5/2}$	6.0739(14)[B]	6.0777			
37 [As]	$4p^3$ [1]	$(4p)_{3/2}$	$4p^24d$ [11]	$((4\overline{p}4p)_1 4\overline{d})_{3/2}$	6.0739(14)[B]	6.0819			
37 [As]	$4p^3$ [2]	$(4\overline{p}(4p^2)_2)_{3/2}$	$4p^24d$ [24]	$((4\overline{p}4p)_1 4d)_{5/2}$	7.2543(16)	7.2153			
37 [As]	$4p^3$ [1]	$(4p)_{3/2}$	$4s4p^4$ [10]	$(4s(4p^2)_2)_{3/2}$	7.3487(12)	7.3232			
37 [As]	$4p^3$ [1]	$(4p)_{3/2}$	$4p^24d$ [8]	$(4d)_{5/2}$	7.5590(12)	7.5369			
37 [As]	$4p^3$ [3]	$(4\overline{p}(4p^2)_2)_{5/2}$	$4p^24d$ [16]	$((4\overline{p}4p)_1 4d)_{7/2}$	8.3091(13)	8.3143			
37 [As]	$4p^3$ [3]	$(4\overline{p}(4p^2)_2)_{5/2}$	$4p^24d$ [14]	$((4\overline{p}4p)_2 4\overline{d})_{7/2}$	8.9027(12)[B]	8.9005			
37 [As]	$4p^3$ [1]	$(4p)_{3/2}$	$4p^24d$ [5]	$(4\overline{d})_{3/2}$	8.9027(12)[B]	8.9011			
37 [As]	$4p^3$ [3]	$(4\overline{p}(4p^2)_2)_{5/2}$	$4p^24d$ [12]	$((4\overline{p}4p)_2 4\overline{d})_{5/2}$	9.2350(13)	9.2406			
37 [As]	$4p^3$ [3]	$(4\overline{p}(4p^2)_2)_{5/2}$	$4s4p^4$ [10]	$(4s(4p^2)_2)_{3/2}$	12.5452(12)	12.4636			
37 [As]	$4p^3$ [2]	$(4\overline{p}(4p^2)_2)_{3/2}$	$4s4p^4$ [7]	$(4s(4p^2)_2)_{5/2}$	14.7125(20)	14.7256			
37 [As]	$4p^3$ [3]	$(4\overline{p}(4p^2)_2)_{5/2}$	$4s4p^4$ [7]	$(4s(4p^2)_2)_{5/2}$	15.6464(13)	15.6883			
37 [As]	$4p^3$ [1]	$(4p)_{3/2}$	$4p^3$ [4]	$(4\overline{p}(4p^2)_0)_{1/2}$	16.2687(13)	16.2531			M1
37 [As]	$4p^3$ [1]	$(4p)_{3/2}$	$4p^3$ [3]	$(4\overline{p}(4p^2)_2)_{5/2}$	17.7347(12)	17.7560			M1
37 [As]	$4p^3$ [1]	$(4p)_{3/2}$	$4p^3$ [2]	$(4\overline{p}(4p^2)_2)_{3/2}$	19.1026(13)	19.1748			M1
38 [Ge]	$4p^2$ [1]	$(4\overline{p}^2)_0$	4p4d [11]	$(4\overline{p}4\overline{d})_1$	5.5873(16)	5.5613		5.5577[a]	
38 [Ge]	$4s4p^3$ [7]	$(4s4p)_1$	4p4f [50]	$(4\overline{p}4\overline{f})_2$	5.7916(16)	5.7877		5.5903[a]	
38 [Ge]	$4p^2$ [1]	$(4\overline{p}^2)_0$	$4s4p^3$ [7]	$(4s4p)_1$	7.4475(12)	7.4283		7.4381[a]	
38 [Ge]	$4s4p^3$ [6]	$(4s4p)_2$	$4s4p^24d$ [25]	$(4s4\overline{d})_2$	8.6742(13)	8.6708		7.4473[a]	
38 [Ge]	$4p^2$ [3]	$(4\overline{p}4p)_2$	4p4d [8]	$(4\overline{p}4\overline{d})_2$	9.1815(12)	9.1981		9.1736[a]	
38 [Ge]	$4p^2$ [2]	$(4\overline{p}4p)_1$	$4s4p^3$ [7]	$(4s4p)_1$	12.4585(12)	12.3827		12.3923[a]	
38 [Ge]	$4p^2$ [3]	$(4\overline{p}4p)_2$	$4s4p^3$ [7]	$(4s4p)_1$	12.9690(12)	12.9046		12.9173[a]	
38 [Ge]	4p4d [8]	$(4\overline{p}4\overline{d})_2$	$4s4p^24d$ [25]	$(4s4\overline{d})_2$	13.7720(13)	13.7643			
38 [Ge]	$4p^2$ [2]	$(4\overline{p}4p)_1$	$4s4p^3$ [6]	$(4s4p)_2$	14.4092(12)	14.4132		14.4352[a]	
38 [Ge]	$4p^2$ [3]	$(4\overline{p}4p)_2$	$4s4p^3$ [6]	$(4s4p)_2$	15.0996(19)	15.1251		15.1525[a]	
38 [Ge]	$4p^2$ [4]	$(4p^2)_2$	$4s4p^3$ [10]	$((4s4\overline{p})_1(4p^2)_2)_3$	15.4766(13)	15.5078		15.5053[a]	
38 [Ge]	$4p^2$ [1]	$(4\overline{p}^2)_0$	$4p^2$ [3]	$(4\overline{p}4p)_2$	17.4834(12)	17.5042		17.5356[a]	E2
38 [Ge]	$4p^2$ [1]	$(4\overline{p}^2)_0$	$4p^2$ [2]	$(4\overline{p}4p)_1$	18.5057(13)	18.5655		18.6055[a]	M1
39 [Ga]	4p [1]	$(4\overline{p})_{1/2}$	4d [8]	$(4\overline{d})_{3/2}$	5.6694(15)	5.6507	5.74[b]	5.608[b]	
								5.6640[c]	
								5.6436[d]	
39 [Ga]	$4s4p^2$ [6]	$((4s4\overline{p})_1 4p)_{3/2}$	4f [30]	$(4\overline{f})_{5/2}$	5.8802(14)	5.8816			
39 [Ga]	4p [1]	$(4\overline{p})_{1/2}$	$4s4p^2$ [7]	$((4s4\overline{p})_1 4p)_{1/2}$	7.3376(12)	7.2995	7.340[b]	7.247[b]	
								7.3309[c]	
								7.2832[d]	
								7.232[e]	

Table 2. Continued.

	Lower level		Upper level		λ_{Present}		$\lambda_{\text{Previous}}$		
Ion	Conf.	State	Conf.	State	Exp.	FAC	Exp.	Theory	Type
39 [Ga]	4p [1]	$(4\overline{p})_{1/2}$	$4s4p^2$ [6]	$((4s4\overline{p})_1 4p)_{3/2}$	7.4528(12)	7.4400	7.45[b]	7.396[b]	
							7.456[b]	7.4506[c]	
								7.4248[d]	
								7.386[e]	
								7.4463[f]	
39 [Ga]	$4s4p^2$ [4]	$((4s4\overline{p})_0 4p)_{3/2}$	4s4p4d [18]	$((4s4\overline{p})_0 4d)_{5/2}$	7.6786(12)[B]	7.6515			
39 [Ga]	$4s4p^2$ [5]	$((4s4\overline{p})_1 4p)_{5/2}$	4s4p4d [21]	$((4s4\overline{p})_1 4d)_{5/2}$	7.6786(12)[B]	7.6653			
39 [Ga]	4p [2]	$(4p)_{3/2}$	$4s4p^2$ [9]	$(4s(4p^2)_2)_{5/2}$	8.3526(23)	8.3797		8.3644[d]	
39 [Ga]	4p [1]	$(4\overline{p})_{1/2}$	$4s4p^2$ [4]	$((4s4\overline{p})_0 4p)_{3/2}$	8.3815(13)	8.4145		8.3982[d]	
39 [Ga]	$4s4p^2$ [5]	$((4s4\overline{p})_1 4p)_{5/2}$	4s4p4d [15]	$((4s4\overline{p})_1 4\overline{d})_{5/2}$	8.9874(13)	8.9983			
39 [Ga]	4p [2]	$(4p)_{3/2}$	$4s4p^2$ [7]	$((4s4\overline{p})_1 4p)_{1/2}$	12.8942(12)	12.7719		12.7177[d]	
39 [Ga]	4p [2]	$(4p)_{3/2}$	$4s4p^2$ [6]	$((4s4\overline{p})_1 4p)_{3/2}$	13.2638(12)	13.2084		13.1556[d]	
39 [Ga]	4p [1]	$(4\overline{p})_{1/2}$	$4s4p^2$ [3]	$(4s)_{1/2}$	14.3034(12)	14.3033		14.2340[d]	
39 [Ga]	4p [2]	$(4p)_{3/2}$	$4s4p^2$ [5]	$((4s4\overline{p})_1 4p)_{5/2}$	15.0147(12)	15.0420		14.9773[d]	
39 [Ga]	4p [2]	$(4p)_{3/2}$	$4s4p^2$ [4]	$((4s4\overline{p})_0 4p)_{3/2}$	16.5265(12)	16.6267		16.5557[d]	
39 [Ga]	4p [1]	$(4\overline{p})_{1/2}$	4p [2]	$(4p)_{3/2}$	17.0124(13)	17.0362		17.0443[d]	M1
								16.9974[g]	
								17.0438[h]	
								17.0153[i]	
								17.0462[i]	
40 [Zn]	4s4p [3]	$(4s4\overline{p})_1$	4s4d [10]	$(4s4\overline{d})_2$	5.7574(15)	5.7515	5.7540(20)[j]	5.7530[j]	
								5.7561[k]	
								5.7561[l]	
								5.7437[m]	
								5.7586[n]	
								5.7437[o]	
40 [Zn]	$4s^2$ [1]	$(4s^2)_0$	4s4p [5]	$(4s4p)_1$	7.3820(12)	7.3470	7.3792(20)[j]	7.3368[j]	
							7.38070(66)[p]	7.3784[j]	
							7.380(2)[q]	7.3790[k]	
								7.3790[l]	
								7.3464[m]	
								7.3824[n]	
								7.3430[o]	
								7.3806[r]	
								7.3684[s]	
								7.38128[t]	
								7.3806[u]	
								7.3816[v]	
								7.38[w]	

Table 2. Continued.

	Lower level		Upper level		λ_{Present}		$\lambda_{\text{Previous}}$		
Ion	Conf.	State	Conf.	State	Exp.	FAC	Exp.	Theory	Type
40 [Zn]	4s4p [4]	$(4s4p)_2$	4s4d [12]	$(4s4d)_2$	7.6810(12)	7.6712		7.6913[j]	
								7.6834[l]	
								7.6553[m]	
								6.9108[n]	
								7.6512[o]	
40 [Zn]	4s4p [4]	$(4s4p)_2$	4s4d [11]	$(4s4d)_3$	7.7372(12)	7.7283	7.7355(20)[j]	7.7049[j]	
								7.7354[j]	
								7.7460[k]	
								7.7460[l]	
								7.7055[m]	
								7.7480[n]	
								7.7013[o]	
40 [Zn]	$4s^2$ [1]	$(4s^2)_0$	4s4p [3]	$(4s4\overline{p})_1$	14.7902(12)	14.6882	14.817(10)[x]	14.7300[j]	
								14.7915[j]	
								14.7949[k]	
								14.7949[l]	
								14.7719[m]	
								14.7879[n]	
								14.7410[o]	
								14.7848[r]	
								14.7984[s]	
								14.7854[u]	
								14.82[w]	
40 [Zn]	4s4p [3]	$(4s4\overline{p})_1$	4s4p [4]	$(4s4p)_2$	18.1448(13)	18.1947		18.1642[j]	M1
								18.1071[l]	
								18.2582[m]	
								18.1267[n]	
								18.2851[o]	
								18.2582[s]	
								18.1508[u]	
41 [Cu]	4p [2]	$(4\overline{p})_{1/2}$	4d [4]	$(4\overline{d})_{3/2}$	5.8262(15)	5.8242	5.824(4)[y]	5.822[y]	
							5.8209(15)[z]	5.8217[aa]	
							5.8190(15)[aa]	5.8184[ad]	
							5.826[ab]	5.8226[ad]	
							5.8265(15)[ac]	5.8239[ae]	
								5.8265[af]	
41 [Cu]	4s [1]	$(4s)_{1/2}$	4p [3]	$(4p)_{3/2}$	7.5871(13)	7.5770	7.5842(15)[z]	7.5712[aa]	
							7.5816(15)[aa]	7.6014[ad]	
							7.59[ab]	7.5866[ad]	
							7.5914(15)[ac]	7.5868[ae]	
							7.58595(47)[ag]	7.5914[af]	

Table 2. Continued.

	Lower level		Upper level		λ_{Present}		$\lambda_{\text{Previous}}$		
Ion	Conf.	State	Conf.	State	Exp.	FAC	Exp.	Theory	Type
							7.585(3)[ah]	7.5839[ah]	
								7.5864[ai]	
								7.5860[aj]	
41 [Cu]	4p [3]	$(4p)_{3/2}$	4d [5]	$(4d)_{5/2}$	8.0778(12)	8.0807	8.0758(15)[z]	8.0704[aa]	
							8.0741(15)[aa]	8.0824[ac]	
							8.084[ab]	8.0615[ad]	
							8.0824(15)[ac]	8.0782[ae]	
41 [Cu]	4d [5]	$(4d)_{5/2}$	4f [7]	$(4f)_{7/2}$	8.2041(12)	8.2039	8.2010(15)[z]	8.2074[aa]	
							8.1991(15)[aa]	8.2147[ad]	
							8.212[ab]		
							8.2077(15)[ac]		
41 [Cu]	4s [1]	$(4s)_{1/2}$	4p [2]	$(4\overline{p})_{1/2}$	14.0949(12)	14.0564	14.0946(15)[z]	14.1114[ad]	
							14.095[ab]	14.0955[ae]	
							14.1089[ac]	14.1089[af]	
								14.0866[ah]	
								14.0955[ai]	
42 [Ni]	$3d^9 4p$ [9]	$(3\overline{d}^3 4\overline{p})_1$	$3d^9 4d$ [35]	$(3\overline{d}^3 4\overline{d})_0$	5.0324(20)	5.0456	5.03(2)[ak]	5.018[ak]	
							5.026(5)[al]	4.980[am]	
								5.024[an]	
42 [Ni]	$3d^9 4p$ [12]	$(3d^5 4p)_1$	$3d^9 4d$ [35]	$(3\overline{d}^3 4\overline{d})_0$	5.6194(15)	5.6394	5.609(5)[al]	5.609[ak]	
								5.557[am]	
								5.611[an]	
42 [Ni]	$3d^9 4p$ [15]	$(3\overline{d}^3 4p)_1$	$3d^9 4d$ [33]	$(3\overline{d}^3 4d)_2$	8.1173(13)	8.1194[A]		8.108[an]	
42 [Ni]	$3d^9 4s$ [4]	$(3\overline{d}^3 4s)_1$	$3d^9 4p$ [8]	$(3\overline{d}^3 4\overline{p})_2$	14.2468(12)[B]	14.2300[A]			
42 [Ni]	$3d^9 4s$ [2]	$(3d^5 4s)_3$	$3d^9 4p$ [6]	$(3d^5 4\overline{p})_2$	14.2468(12)[B]	14.2616[A]			
42 [Ni]	$3d^9 4s$ [3]	$(3d^5 4s)_2$	$3d^9 4p$ [7]	$(3d^5 4\overline{p})_3$	14.3475(13)	14.3326[A]			
42 [Ni]	$3d^9 4s$ [5]	$(3\overline{d}^3 4s)_2$	$3d^9 4p$ [8]	$(3\overline{d}^3 4\overline{p})_2$	14.4236(13)	14.4146[A]			
42 [Ni]	$3d^9 4s$ [3]	$(3d^5 4s)_2$	$3d^9 4p$ [6]	$(3d^5 4\overline{p})_2$	14.5253(13)	14.5308[A]			

Note: 1. Superscripts A and B represent the wavelengths from RMBPT [46] and blended lines, respectively.

2. References: [a] [50]; [b] [9]; [c] [51]; [d] [53]; [e] [76]; [f] [52]; [g] [54]; [h] [55]; [i] [56]; [j] [26]; [k] [62]; [l] [60]; [m] [65]; [n] [58]; [o] [64]; [p] [24]; [q] [30]; [r] [57]; [s] [66];[t] [59]; [u] [63]; [v] [61]; [w] [67]; [x] [34]; [y] [12]; [z] [27]; [aa] [28] [ab] [29]; [ac] [31]; [ad] [68]; [ae] [69]; [af] [72]; [ag] [25]; [ah] [33]; [ai] [70]; [aj] [71]; [ak] [35]; [al] [36]; [am] [74]; [an] [75].

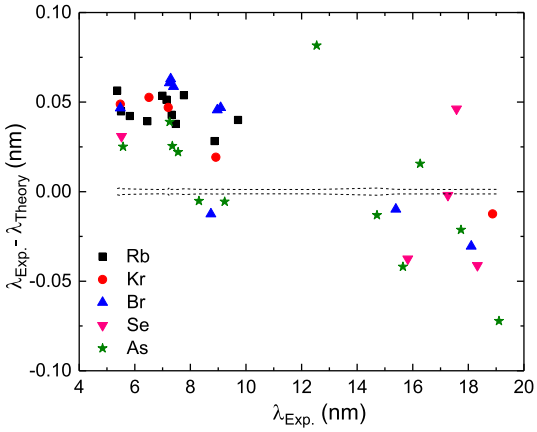

Figure 3. Difference between FAC and experimental wavelengths (in nm) for $n = 4$–4 transitions in Rb-like to As-like Yb ions. The dashed line represents the experimental uncertainties of each line as listed in table 2.

later improved their calculations by including frequency-dependent, retarded Breit corrections and QED calculations [61], while Safronova and Safronova [62] used the same approach but without QED corrections. The two results [60, 62] produced the same wavelengths when QED effects were not included, and the QED contribution to the resonance transition is about 0.0026 nm. Chen and Cheng [63] carried out a relativistic configuration interaction calculation which included QED corrections. Other work includes calculations within MCDF [64], GRASP [65, 66], and Hebrew University-Lawrence Livermore Atomic code (HULLAC) [26]. Additionally, the Dirac–Fock and semi-empirical methods have been used by Curtis [67].

The measured and calculated wavelengths are listed in table 2, and the resonance transition is compared in figure 4. The recommended wavelength of 7.3808(5) nm, shown in the same figure, was calculated using the measured wavelengths weighted by their uncertainties. As can be seen in the figure, the measured wavelengths are in very good agreement with the recommended value. The calculations of Hao and Liu [57], Träbert *et al* [59], Blundell [61], Chen and Cheng [63], and semi-empirical calculations of Curtis [67] are in excellent agreement with the recommended wavelength. The results of Vilkas and Ishikawa [58], Safronova and Safronova [62], and Blundell *et al* [60] are also comparable to the measured wavelength. Similar agreement between theoretical results and measured wavelengths is observed for other transitions. Our measured wavelength of 14.7902(12) nm for the $(4s^2)_0 - (4s4\overline{p})_1$ transition showed significant difference from the PLT tokamak [34] results. However, the predicted wavelength based on the semi-empirical fitting along the isoelectronic sequence and the theoretical results [57, 58, 60, 62, 63] support the present measured wavelength.

4.5. Cu-like Yb^{41+}

The strong lines due to the 4s–4p resonance transition and the 4s–4$\overline{p}$ transition in Cu-like Yb are readily identified for $E_b \geqslant 2.21$ keV, which is slightly greater than its ionization energy. In

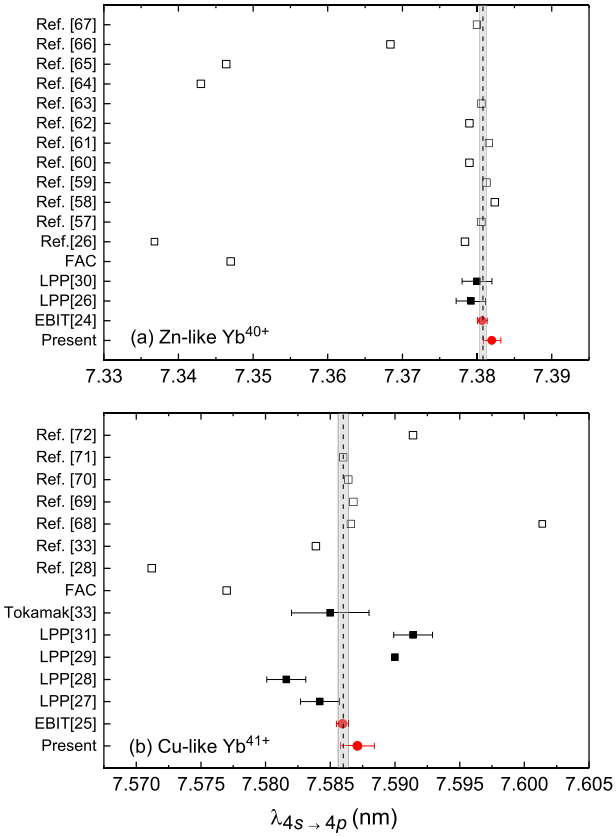

Figure 4. Comparison of the present measured wavelength with the previously reported experimental and theoretical values for the resonance transition 4s–4p in (a) Zn-like (b) Cu-like Yb ions. Solid circles (red) and squares (black) represent the EBIT and laser-produced plasma measurements, respectively. Open squares present the theoretical wavelengths. The dashed line is the recommended wavelength of the resonance transition, and the shaded region presents the bounds of the uncertainty.

addition, the other lines between the excited states due to the $4\overline{p} - 4\overline{d}$, 4p–4d, and 4d–4f transitions are also observed in the measured spectra. The wavelengths of the identified transitions are listed in table 2 along with their comparison to the previous reported values [12, 25, 27–29, 31, 33, 68–72]. A vast amount of literature exists on the wavelengths of the five lines observed in the Cu-like isoelectronic sequence of the present spectra. This is because the atomic system with one-valence electron in the outer shell makes the study of spectra easier than that for multi-valence electrons. Also, it provides the benchmark data to test atomic structure theories [70, 73].

A comparison of our measured wavelength of the resonance transition with previously reported values is shown in figure 4(b). Although our measurement of 7.5871(13) nm has a larger uncertainty, it agrees with the most recent EBIT-measured value of 7.58595(47) nm by Utter *et al* [25]. Both the EBIT and the PLT tokamak [33] results agree with the recommended wavelength of 7.5860(4) nm. The difference between the EBIT and LPP [28, 29, 31] data may be attributed to self-absorption and high-density effects. The other observed lines were measured only in laser-produced plasmas [27–29, 31] except for the $4\overline{p} - 4\overline{d}$ transition, which was reported recently by Suzuki *et al* [12] from LHD. Our measured

wavelength of 5.8262(15) nm agrees with their value of 5.824(4) nm within the mutual uncertainties but has better accuracy.

In regards to theory, several calculations [12, 28, 31, 68–72] have been published for Cu-like ions. Here, we mention three state-of-the-art calculations following an accurate QED correction in addition to relativistic and electron correlation effects. Cheng and Chen [69] employed RMBPT with QED corrections calculated with Dirac–Kohn–Sham potentials to account for screening and core-relaxation effects. Blundell [70] carried out *ab initio* calculations of the screened self-energy and vacuum polarization to incorporate the QED effects. Kim *et al* [71] calculated QED energies by adjusting hydrogenic values with the Welton method to account for screening corrections. It can be seen from figure 4 that their predictions are in excellent agreement with the recommended wavelength of the resonance transition. Comparison of our measured values for the other observed transitions with these calculations have similar agreement. Palmeri *et al* [68] have reported a wavelength of 7.6014 nm for the same transition using the GRASP code, and their adjusted wavelength of 7.5866 nm is in agreement with the recommended value.

4.6. Ni-like Yb^{42+}

Two spectral lines due to the $(3\overline{d}^3 4\overline{p})_1$–$(3\overline{d}^3 4\overline{d})_0$ and $(3d^5 4p)_1$–$(3\overline{d}^3 4\overline{d})_0$ transitions are identified in our measured spectra. Wavelength measurements for these two lines were reported previously in spectra from LPPs to explore the soft x-ray lasing in Ni-like heavy elements [35, 36]. The wavelengths measured by Daido *et al* [35] and MacGowan *et al* [36] are shorter than the present results and have larger uncertainties of 0.02 nm and 0.005 nm, respectively. In the 14 nm–15 nm range, four new lines from the $3d^9 4s$–$3d^9 4p$ transitions are observed in our measured spectra, while five new lines are predicted. The comparison of the measured and calculated intensity ratios of the lines at 14.2468 nm and 14.3475 nm confirms line blending.

As mentioned earlier, the energies of the $3d^9 4l$ configuration having total angular momentum $J = 1$–3 are taken from the RMBPT calculations [46] in the model. However, there are no RMBPT results available for $J = 0$ level, and the difference between the presented theoretical and experimental wavelengths is less than 0.4% for the transition involving the $J = 0$ level. RMBPT results agree at a level of 0.03%–0.12% with the measured wavelengths. Other theoretical results include the work of Daido *et al* [35], Ivanova [74], and Scofield and MacGowan [75]. Daido *et al* [35] used the GRASP code including Breit and quantum electrodynamics (QED) corrections. Ivanova [74] carried out calculations using relativistic perturbation theory with a zero-approximation model potential for Ni-like isoelectronic sequence. Scofield and MacGowan [75] performed calculations within the relativistic multi-configuration Hartree–Fock approach. Daido *et al* [35] and Scofield and MacGowan [75] calculations show very good agreement on the order of 0.3% and 0.2%, respectively, with the observed wavelengths.

5. Conclusions

EUV emission recorded with a high-resolution flat-field grazing incidence spectrometer was analyzed with the detailed collisional-radiative model using the NOMAD code. The measured spectra revealed features arising due to strong mixing through configuration interaction that were taken into account in the CR model. In this work, we report wavelengths for 94 lines which were identified by comparing the measured spectra with theoretical line positions and intensities. These lines are due to $n = 4$–4 transitions in Rb-like to Ni-like Yb ions. Seventy-nine lines are reported for the first time, while our measured wavelengths of 15 previously-observed lines are found to have better accuracy except for the resonance transitions in Zn-like and Cu-like Yb ions [24, 25]. Our measured wavelengths are in excellent agreement with the few high-accuracy calculations that include electron correlation, Breit, and QED effects. These are available for a few lines in the Cu-like and Zn-like atomic systems. The present measurements provide benchmark data to test the high-accuracy calculations in atomic systems with multi-valence electrons.

Acknowledgments

This work was partially funded by the NIST Grant Award Numbers 70NANB16H204, 70NANB18H284, and 70NANB19H024 of the Measurement Science and Engineering (MSE) Research Grant Programs, and by the National Science Foundation Award Number 1806494. JMD acknowledges funding from a National Research Council Postdoctoral Fellowship.

ORCID iDs

Dipti https://orcid.org/0000-0001-6675-8509
J M Dreiling https://orcid.org/0000-0001-9226-203X
Yu Ralchenko https://orcid.org/0000-0003-0083-9554

References

[1] Wollaeger R T, Korobkin O, Fontes C J, Rosswog S K, Even W P, Fryer C L, Sollerman J, Hungerford A L, Van Rossum D R and Wollaber A B 2018 *Mon. Not. R. Astron. Soc.* **478** 3298–334
[2] O'Sullivan G, Li B, D'Arcy R, Dunne P, Hayden P, Kilbane D, McCormack T, Ohashi H, O'Reilly F, Sheridan P, Sokell E, Suzuki C and Higashiguchi T 2015 *J. Phys. B: At. Mol. Opt. Phys.* **48** 144025
[3] Marcus G, Louzon E, Henis Z, Maman S and Mandelbaum P 2007 *J. Opt. Soc. Am.* B **24** 1187–92
[4] Churilov S S, Kildiyarova R R, Ryabtsev A N and Sadovsky S V 2009 *Phys. Scr.* **80** 045303
[5] Otsuka T, Kilbane D, White J, Higashiguchi T, Yugami N, Yatagai T, Jiang W, Endo A, Dunne P and O'Sullivan G 2010 *Appl. Phys. Lett.* **97** 111503
[6] Otsuka T, Kilbane D, Higashiguchi T, Yugami N, Yatagai T, Jiang W, Endo A, Dunne P and O'Sullivan G 2010 *Appl. Phys. Lett.* **97** 231503

[7] Sheil J, Dunne P, Higashiguchi T, Kos D, Long E, Miyazaki T, O'Reilly F, O'Sullivan G, Sheridan P, Suzuki C, Sokell E, White E and Kilbane D 2017 *J. Phys. B: At. Mol. Opt. Phys.* **50** 065006

[8] Träbert E, Beiersdorfer P, Hell N and Brown G V 2015 *Phys. Rev.* A **92** 022509

[9] Fournier K B, Goldstein W H, Osterheld A, Finkenthal M, Lippmann S, Huang L K, Moos H W and Spector N 1994 *Phys. Rev.* A **50** 2248

[10] Suzuki C *et al* 2014 *Phys. Scr.* **89** 114009

[11] Suzuki C, Koike F, Murakami I, Tamura N and Sudo S 2015 *J. Phys. B: At. Mol. Opt. Phys.* **48** 144012

[12] Suzuki C, Koike F, Murakami I, Tamura N and Sudo S 2018 *Atoms* **6** 24

[13] Gillaspy J D 1997 *Phys. Scr.* **T71** 99–103

[14] Ratliff L and Roberts J 2001 *Highly Charged Ion Studies at the NIST EBIT, Trapping Highly Charged Ions: Fundamentals and Applications* (Hauppauge, NY: Nova Science Publishers)

[15] Kilbane D, O'Sullivan G, Gillaspy J D, Ralchenko Y and Reader J 2012 *Phys. Rev.* A **86** 042503

[16] Kilbane D, Gillaspy J D, Ralchenko Y, Reader J and O'Sullivan G 2013 *Phys. Scr.* **T156** 014012

[17] Kilbane D, O'Sullivan G, Podpaly Y A, Gillaspy J D, Reader J and Ralchenko Y 2014 *Eur. Phys. J.* D **68** 222

[18] Podpaly Y A, Gillaspy J D, Reader J and Ralchenko Y 2015 *J. Phys. B: At. Mol. Opt. Phys.* **48** 25002

[19] Kobayashi T, Akamatsu D, Hisai Y, Tanabe T, Inaba H, Suzuyama T, Hong F L, Hosaka K and Yasuda M 2018 *IEEE Trans. Ultrason. Ferroelectrics Freq. Contr.* **65** 2449–58

[20] Hinkley N, Sherman J A, Phillips N B, Schioppo M, Lemke N D, Beloy K, Pizzocaro M, Oates C W and Ludlow A D 2013 *Science* **341** 1215–8

[21] Chipaux R, Cribier M, Dujardin C, Garnier N, Guerassimova N, Mallet J, Meyer J P, Pédrini C and Petrosyan A G 2005 *Nucl. Instrum. Methods Phys. Res.* A **486** 228–33

[22] Fan T, Ripin D J, Aggarwal R L, Ochoa J R, Chann B, Tilleman M and Spitzberg J 2007 *IEEE J. Sel. Top. Quantum Electron.* **65** 448–59

[23] Träbert E, Beiersdorfer P and Chen H 2004 *Phys. Rev.* A **70** 032506

[24] Utter S B, Beiersdorfer P and Träbert E 2003 *Can. J. Phys.* **81** 911–8

[25] Utter S B, Beiersdorfer P, Träbert E and Clothiaux E J 2003 *Phys. Rev.* A **67** 032502

[26] Brown C M, Seely J F, Kania D R, Hammel B A, Back C A, Lee R W, Bar-Shalom A and Behring W E 1994 *At. Data Nucl. Data Tables* **58** 203–17

[27] Kania D R, MacGowan B J, Keane C J, Brown C M, Ekberg J O, Seely J F, Feldman U and Reader J 1990 *J. Opt. Soc. Am.* B **7** 1993–6

[28] Doschek G A, Feldman U, Brown C M, Seely J F, Ekberg J O, Behring W E and Richardson M C 1988 *J. Opt. Soc. Am.* B **5** 243–6

[29] Finkenthal M, Moos H W, Bar Shalom A, Spector N, Zigler A and Yarkoni E 1988 *Phys. Rev.* A **38** 288–95

[30] Acquista N and Reader J 1984 *J. Opt. Soc. Am.* B **1** 649–51

[31] Reader J and Luther G 1981 *Phys. Scr.* **24** 732–7

[32] Reader J and Luther G 1980 *Phys. Rev. Lett.* **45** 609–13

[33] Seely J F, Feldman F, Wouters A W, Schwob J L and Suckewer S 1989 *Phys. Rev.* A **40** 5020–5

[34] Hinnov E, Beiersdorfer P, Bell R, Stevens J, Suckewer S, von Goeler S, Wouters A, Dietrich D, Gerassimenko M and Silver E 1987 *Phys. Rev.* A **35** 4876–7

[35] Daido H, Ninomiya S, Takagi M, Kato Y and Koike F 1999 *J. Opt. Soc. Am.* B **16** 296–300

[36] MacGowan B J, Maxon S, Hagelstein P L, Keane C J, London R A, Matthews D L, Rosen M D, Scofield J H and Whelan D A 1987 *Phys. Rev. Lett.* **59** 2157–60

[37] Kramida A 2019 NIST atomic energy levels and spectra bibliographic database (version 2.0) https://physics.nist.gov/Elevbib

[38] Fahy K, Sokell E, O'Sullivan G, Aguilar A, Pomeroy J M, Tan J N and Gillaspy J D 2007 *Phys. Rev.* A **75** 032520

[39] Holland G E, Boyer C N, Seely J F, Tan J N, Pomeroy J M and Gillaspy J D 2005 *Rev. Sci. Instrum.* **76** 073304

[40] Silwal R, Takacs E, Dreiling J M, Gillaspy J D and Ralchenko Y 2017 *Atoms* **5** 30

[41] Blagojević B, Le Bigot E O, Fahy K, Aguilar A, Makonyi K, Takacs E, Tan J N, Pomeroy J M, Burnett J H, Gillaspy J D and Roberts J R 2005 *Rev. Sci. Instrum.* **76** 083102

[42] Osin D, Reader J, Gillaspy J D and Ralchenko Y 2012 *J. Phys. B: At. Mol. Opt. Phys.* **45** 0245001

[43] Ralchenko Y and Maron Y 2001 *J. Quant. Spectrosc. Radiat. Transfer* **71** 609–21

[44] Gu M F 2008 *Can. J. Phys.* **86** 675–89

[45] Draganić I N, Ralchenko Y, Reader J, Gillaspy J D, Tan J N, Pomeroy J M, Brewer S M and Osin D 2011 *J. Phys. B: At. Mol. Opt. Phys.* **44** 025001

[46] Safronova U I, Safronova M S and Beiersdorfer B 2007 *J. Phys. B: At. Mol. Opt. Phys.* **40** 955–74

[47] Ralchenko Y, Draganic I N, Tan J N, Gillaspy J D, Pomeroy J M, Reader J, Feldman U and Holland G E 2013 *Phys. Rev.* A **88** 012506

[48] Jönsson P, Gaigalas G, Bieroń J, Fischer C F and Grant I P 2013 *Comput. Phys. Commun.* **184** 2197–203

[49] Mandelbsum P, Seely J F, Bar-Shalom A and Klapisch M 1991 *Phys. Rev.* A **44** 5744–51

[50] Palmeri P, Quinet P, Biémont É and Träbert E 2007 *At. Data Nucl. Data Tables* **93** 355–74

[51] Fan J Z, Zhang D H, Chang Z W, Shi Y L and Dong C Z 2012 *Chin. Phys. Lett.* **29** 073102

[52] Hu F, Yang J M, Wang C K, Jing L F, Chen S B, Jiang G, Liu H and Hao L H 2011 *Phys. Rev.* A **84** 042506

[53] Quinet P, Biémont É, Palmeri P and Träbert E 2007 *At Data Nucl. Data Tables* **93** 167–82

[54] Safronova U I, Cowan T E and Safronova M S 2006 *Phys. Lett.* A **348** 293–8

[55] Ali M A 1997 *Phys. Scr.* **55** 159–66

[56] Curtis L J 1987 *Phys. Rev.* A **35** 2089–94

[57] Hao L H and Liu J J 2018 *J. Appl. Spectrosc.* **85** 730–7

[58] Vilkas M J and Ishikawa Y 2005 *Phys. Rev.* A **72** 032512

[59] Träbert E, Clementson J, Beiersdorfer P, Santana J A and Ishikawa Y 2011 *Can. J. Phys.* **89** 639–45

[60] Blundell S A, Johnson W R, Safronova M S and Safronova U I 2008 *Phys. Rev.* A **77** 032507

[61] Blundell S A 2009 *Can. J. Phys.* **87** 55–65

[62] Safronova U I and Safronova M S 2010 *J. Phys. B: At. Mol. Opt. Phys.* **43** 074025

[63] Chen M H and Cheng K T 2010 *J. Phys. B: At. Mol. Opt. Phys.* **43** 074019

[64] Biémont É 1984 *At. Data Nucl. Data Tables* **1** 163–244

[65] Quinet P, Biémont É, Palmeri P and Träbert E 2007 *At. Data Nucl. Data Tables* **93** 711–29

[66] Hu F, Jing G, Yang J M, Wang C K, Zhao X F and Hao L H 2011 *Eur. Phys. J.* D **61** 15–20

[67] Curtis L J 1992 *J. Opt. Soc. Am.* B **5** 5–9

[68] Palmeri P, Quinet P, Biémont É and Träbert E 2007 *At. Data Nucl. Data Tables* **93** 537–47

[69] Chen M H, Cheng K T, Johnson W R and Sapirstein J 2006 *Phys. Rev.* A **74** 042510

[70] Blundell S A 1993 *Phys. Rev.* A **47** 1790–803

[71] Kim Y K, Baik D H, Indelicato P and Desclaux J P 1991 *Phys. Rev.* A **44** 148–66

[72] Curtis L J and Theodosiou C E 1989 *Phys. Rev.* A **39** 605–15
[73] Gillaspy J D, Osin D, Ralchenko Y, Reader J and Blundell S A 2013 *Phys. Rev.* A **87** 062503
[74] Ivanova E P 2015 *Opt. Spectrosc.* **118** 506–12
[75] Scofield J H and MacGowan B J 1992 *Phys. Scr.* **46** 361–4
[76] Zilitis V A 1996 *Opt. Spectrosc.* **81** 433–86